Vol. 16, No. 3 (2017) 1029-1052
Revista Mexicana de Ingeniería Química

ANALYSIS OF OPERATING CONDITIONS FOR CANE SUGAR BATCH CRYSTALLIZATION BASED ON MSZW COUPLED WITH MECHANISTIC KINETIC MODELS

ANÁLISIS DE LAS CONDICIONES DE OPERACIÓN PARA LA CRISTALIZACIÓN POR LOTES DE AZÚCAR DE CAÑA BASADA EN MSZW ACOPLADA CON MODELOS CINÉTICOS MECANÍSTICOS

K.B. Sánchez-Sánchez, E. Bolaños-Reynoso*, G.R. Urrea-García
División de Estudios de Posgrado e Investigación, Instituto Tecnológico de Orizaba-TecNM. Avenida Oriente 9 Núm. 852 Colonia Emiliano Zapata. Orizaba, Veracruz, México, 94320.
Received April 27, 2017; Accepted June 30, 2017

Abstract

This work presents the improvement of vacuum pressure and total evaporation time based on the metastable zone width (MSZW) and crystallization kinetics. An approach of fractional feeding was used in a cane sugar batch crystallizer at pilot-scale plant, operating condition imposed in the cane sugar industrial crystallization. The MSZW was used as a strategy to limit the concentration within the saturation and metastable curves. It was coupled with a detailed analysis for primary nucleation and crystal growth, based on mechanistic kinetic models. The more efficient strategy for the fractional feeding increase D(4,3) to 1089.51 μm avoiding losses of FCM (4,700.98 gr) at final process time of 90 min.
Keywords: batch crystallization, MSZW approach, cane sugar, crystallization kinetics, fractional feeding.

Resumen

Este trabajo presenta el mejoramiento de la presión de vacío y el tiempo total de evaporación basado en la amplitud de la zona metaestable (MSZW) y cinéticas de cristalización. Un enfoque de alimentación fraccionada fue usado en la cristalización por lotes de azúcar de caña a escala planta piloto, condiciones de operación semejantes a las empleadas en la cristalización de azúcar de caña a nivel industrial. La MSZW fue usada como una estrategia para limitar la concentración dentro de las curvas de saturación y metaestable. Fue acoplado un análisis detallado para la nucleación primara y crecimiento de cristal, basado en modelos cinéticos mecanísticos. La estrategia más eficiente para la alimentación fraccionada incrementa la D(4,3) hasta 1,089.51 μm, evitando perdidas de FCM (4,700.98 gr) en el tiempo final de proceso de 90 min.
Palabras clave: cristalización por lotes, enfoque MSZW, azúcar de caña, cinéticas de cristalización, alimentación fraccionada.

1 Introduction

Batch crystallization from solution is a key unit operation and the most effective approach for the isolation and/or purification of fine chemical products and intermediates in pharmaceutical, agrochemical, biochemical, petrochemical, and food industries (Hojjati *et al*., 2007; Aamir *et al*., 2010; Kalbasenka *et al*., 2011; Nagy *et al*., 2012). This is often the preferred operation for multi-product plants with a low-volume production capacity and high-value end products (Hu *et al*., 2005; Binev *et al*., 2015), and offers several advantages over others separation techniques such as low operation costs, high-purity (crystalline) products in a single (solid) stage and attractive final product appearance for commercial purposes. The main operational challenge in these processes is to increase the productivity while satisfying the product quality requirements such as purity, shape, size, habit, morphology, as well as batch reproducibility requirements (Aamir *et al*., 2010; Mesbah *et al*., 2010; Mesbah *et al*., 2012).

Typically, the main objective of batch crystallization is to produce a uniform and reproducible crystal size distribution (CSD), which results from the competition between nucleation and growth rate (Damour *et al*., 2011). CSD can be described by the crystal average diameter (% volume D(4,3)) and its standard deviation S(4,3), where large D(4,3) with narrow S(4,3) is desired to simplify downstream processes like washing, filtration

* *Corresponding author. E-mail*: eusebio.itorizaba@gmail.com

and drying (Qamar *et al*., 2011; Mitchell *et al*., 2011). Such crystal properties are directly affected by operational aspects including the time at which the crystal seed is introduced into the batch, its characteristic CSD, the agitation rate (Kim *et al*., 2002; Kalbasenka *et al*., 2004; Akrap *et al*., 2010, Ni *et al*., 2010; Sander *et al*., 2012; Chianese and Kramer, 2012; Bolaños *et al*., 2014), and the imposed cooling temperature-trajectory amongst others (Bolaños *et al*., 2000; Bolaños *et al*., 2008). As discussed in Aamir *et al*., (2010) most batch crystallization processes involve seeding, that varies from as low as 0.5 to as high as 10 in mass %, depending on the size and volume of the batch crystallizer. Seeding techniques are widely accepted to produce more uniform and consistent CSD, provided that uniform seed with high quality of crystal seed with narrow and specific CSD is used (Braatz R., 2002; Braatz and Hasebe, 2002; Hermanto *et al*., 2007; Kim *et al*., 2013; Wang *et al*., 2015).

The Formed Crystal Mass (FCM), also referred as the yield at the cane sugar industrial crystallization (Bolaños *et al*., 2008; Bolaños *et al*., 2014), is another performance measure mainly used in batch crystallization that depends on the cooling temperature trajectory, the vacuum pressure profile and the properties of the crystal seed introduced into the batch. Both the FCM and the CSD are dominated by physicochemical phenomena such as nucleation, growth and agglomeration of crystals which arise from the presence of a co-continuous phase and a dispersed phase (Mesbah *et al*., 2012).

Interest in the optimal operation of cane sugar batch crystallization processes has substantially grown in recent years, highly encouraged by the critical need to satisfy the specifications on purity, crystal size and shape distribution (Choong and Smith, 2004; Sarkar *et al*., 2006; Bolaños *et al*., 2014). However, the cane sugar crystallization from an industrial process viewpoint is not yet understood and has been rarely studied before. Velazquez *et al*., (2010) developed an automated image analysis tool for quality evaluation and inspection of food (cane sugar crystals) processes and products using Fourier analysis fractal dimension and lacunarity. Bolaños *et al*., (2008) reported the applications of natural, exponential and cubic cooling temperature-trajectories with the aim to increase the D(4,3) and FCM, with the natural trajectory promoting higher D(4,3) and FCM compared with strategies reported previously. Quintana *et al*., (2008) presented a first study on the analysis of two different approaches to modeling the crystallization kinetics based of an empirical power law type equations model and a mechanistic framework (Theoretical models). They reported that cane sugar crystallization is dominated by the integration rate. Suarez *et al*., (2011) developed a nonlinear model predictive control (NLMPC) strategy for the operation of industrial fed-batch multi-stage sugar crystallization processes. The results demonstrate that the NLMPC leads to improved end point process specifications, when compared with a proportional-integral (PI) controller. Bolaños *et al*., (2014) presents a study about dynamic modelling and agitation rate optimization for cane sugar crystallization, it was shown that agitation rate has a significant effect on the dynamic evolution of CSD, allowing to achieve specific requirements and reduce the overall time process. However, the operation of cane sugar crystallization still heavily relies upon operators' experience and can significantly differ from an operator to another, with a decrease in the industrial process performance and the final product quality. Due to the factors discussed above, industrial crystallization becomes a wide area of opportunities for research purposes.

Usually, the cane sugar crystallization operation focuses on the supersaturation (Sr) control, which is known to be driving force for the nucleation, growth of crystals. The relative contribution of these can be optimized if Sr is kept into the first metastable zone width (MSZW), located between the solubility and the nucleation curve (Hojjati *et al*., 2007). Since Sr is a direct function of the crystallizer's temperature, the slurry temperature is often used as the manipulated variable to maintain the system in state of supersaturation. Most of applied control approaches are performed through the implementation of time-dependent temperature profiles that aim to maintain the system within the first metastable zone. The temperature profiles are calculated based on the use of trial and error experimentation (Quintana *et al*., 2004; Bolaños *et al*., 2008), mathematical modeling analysis (Hu *et al*., 2005; Nagy *et al*., 2008; Mesbah *et al*., 2010) and the direct design approach (Nagy *et al*., 2009; Fujiwara *et al*., 2005). Although the efforts made in this area, the identification of optimal operating conditions for the key variables involved in the cane sugar industrial process, e.g., temperature-trajectory, vacuum pressure profile and total evaporation time, are not well stablished and remains an active area of research.

This work presents reports the improvement of vacuum pressure and total evaporation time based on the metastable zone width (MSZW) and crystallization kinetics (nucleation and growth). The new approach

is the use of a fractional feeding strategy in a cane sugar pilot-scale batch crystallizer, that is like those operating conditions imposed in the cane sugar industrial crystallization. A factorial experimental design, with eight experiments (runs and replicates) to ensure the degrees of freedom in the statistical analysis was applied to optimize the vacuum pressure and total evaporation time to maintain the concentration close to the saturation curve (e.g., $Sr \rightarrow 0$), maximizing D(4,3) and avoiding losses of formed crystal mass (FCM).

In addition, an industrial database was used to evaluate the impact of the results from the factorial experimental design to compare the current industrial approach with the new approach using the fractional feeding strategy and the improved of vacuum pressure and total evaporation time. Agitation rate was kept constant at 250 rpm to avoid the attrition and agglomeration phenomena (Bolaños *et al*., 2014). Also, it has not effect on the MSZW for cane sugar crystallization (Sánchez *et al*., 2015). To the authors' knowledge, this is the first study related to cane sugar industrial crystallization to reports an in-depth analysis of the key process variables effects into the MSZW under a fractional feeding policy. Additionally, analysis of primary nucleation and crystal growth is incorporated, based on a theoretical mathematical framework to gain knowledge at the microscopic scale. The experiments were conducted at pilot-scale plant; the best results were applied in an industrial crystallizer, operated under the same strategy of fractional feeding policy. The insight acquired from the results of this paper are of high impact for the cane sugar industry, allowing the process to operate efficiently, increasing the overall performance, reducing energy consumption and environmental impact.

2 Experimental equipment

2.1 Pilot-scale batch crystallizer

Figure 1 shows a schematic set-up of the pilot-scale batch crystallizer used in the experimental stage. A brief description of the experimental set-up is presented in Table 1, and included a stainless steel batch crystallizer (pilot plant) with a heating-cooling jacket, steam generator, DC motor, vacuum pump, a direct contact condenser, a slurry trap and a tachometer that indicates the agitation rate.

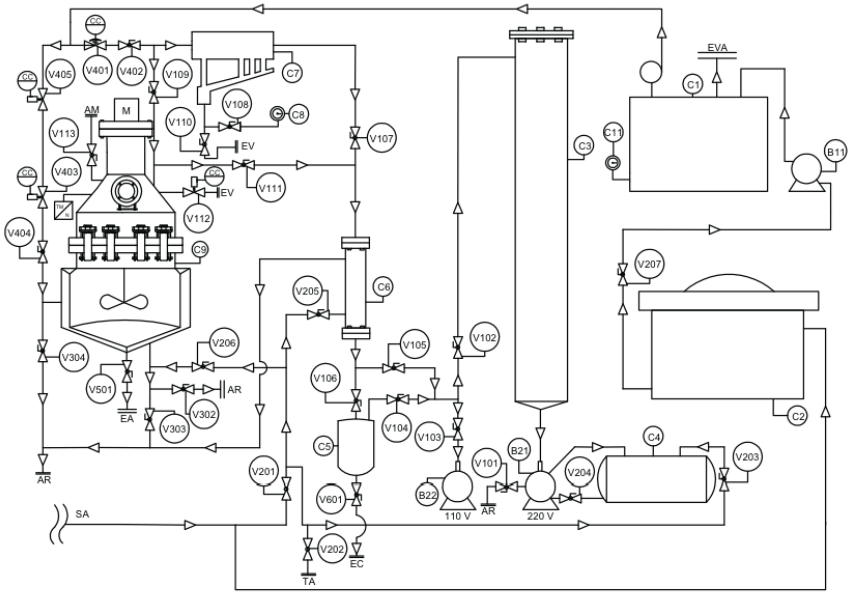

Fig. 1. Experimental pilot-scale batch crystallizer

Table 1. Devices of the experimental pilot-scale batch crystallizer

Quantity	Device
1	DMA 4500 (high resolution with 1e-05 of significant figures) density measuring module, based on the proven oscillating U-tube principle ensuring highly accurate density values.
2	J type thermocouple, temperature of 0-760 ºC, cable length 1 m.
2	Thermowells. Stainless steel.
1	Vacuum pump Felisa FE-1400, 0.3 HP.
1	Proportional control solenoid valve, Burkert. Average temperature of 140 ºC, with digital controller.
6	2-way solenoid valve, normally closed, steel, Parker.
6	Flow valve to allow water and steam flow through pipes.
1	Pressure regulator Norgren Mexico.
1	Vacuum pressure transmitter. Cole-Parmer Model 07356-11. Stainless Steel.
2	Pressure transmitter, Cole-Parmer Model 68072-08.
1	Steam boiler, model MBA9 of SUSSMAN; maximum pressure, 100 Psi; work voltage, 240 VAC; control voltage, 120 VAC.
1	Hydraulic pump, QB60 Clean Water Pump, 1.5 HP.
1	Galvanized pipe system for water circulation.
1	High temperature insulation system.
1	Manometer, ASHCROFT.
1	Condenser, stainless steel surface.
1	Plastic tank 1100 L capacity.
1	Stainless steel crystallizer of 12.77 L, heating-cooling jacket of 11.10 L, four vertical wall baffles of 17 cm (wide) by 3.5 cm (length), agitation arrow of 39 cm (length).
1	Agitator for closed tank, model NSDB of HP, direct transmission of 1750 rpm (1 phase, 60 cycles), 110 VCA totally closed, without ventilation, stainless steel 316 with bridle of 4 in. (diameter) in stainless steel, with agitating arrow of 26 in. (length) and 1/2 in. of diameter in stainless steel 316; velocity investor (driver) integrated with rank from 0 to 1750 rpm
1	Marine propeller type impeller.
1	Programmable tachometer. Range from 50 to 999,990 rpm.
1	Optical sensor for distances of 3 ft. Range 1 – 150000 rpm.
1	Microscope trinocular 48923-30 Cole-Parmer.
1	Monochrome camera with RS-170, video lens with 0.19 mm per pixel.
1	PC, Intel Pentium IV. Operating system XP, 4 GB RAM memory, hard disc of 1 TB
4	Data acquisition card (NI PCI-6023E, NI PCI-6025E, NI PCI-6711 and NI PCI-232/2). Analogic-digital and digital-analogic converters allow the input/output analogic and digital signals.
2	Signal conditioning module (NI SCC-TC02).
1	Image acquisition card (NI PCI-1409).
1	Galvanized steel condenser of direct contact with 2.27 m high and 0.3 m of diameter.

The studies reported by Bolaños *et al*., (2008) and Bolaños *et al*., (2014) provides a detailed description of all the equipment and instrumentation devices installed in the pilot plant. The operation procedure of the batch crystallization pilot-scale plant is described next.

The traditional operation cycle of the industrial cane-sugar crystallization is divided in many sequential phases. During the first stage, the crystallizer is partially filled with a juice that contains dissolved sugar, which is called mother liquor. Evaporation is applied to concentrate the liquor to obtain a preset supersaturation value. Here, crystals seeds are introduced to induce their growth at low levels of supersaturation and to reduce the effect of spontaneous nucleation (primary). In the second

phase, the water is evaporated with a constant vacuum pressure and the concentration of dissolved dry sucrose (density) in mother liquor increases, producing the crystal growth. In the standard vacuum crystallization process, the evaporation takes place and it is necessary to add more mother liquor or hot water to maintain a good level of the supersaturation, increasing the volume. The third phase, consists of controlling the evaporation capacity. At the end of the process, the crystallizer is full of a sugar crystal suspension and final molasses (slurry) that are dropped in a storage tank before being centrifuged. The current crystallizer control involves the manipulation of feed velocity of sugar liquor and syrup, keeping up constant the vacuum pressure for a larger number of batch process (Bolaños *et al*., 2008).

The operation strategy proposed in this work begins with the loading of the saturated sugar solution (1.3594 - 1.3614 g/cm^3 at 70 ºC) into the crystallizer. In case the solution is unsaturated, solvent (water) must be evaporated to reach the saturation concentration by adding steam into the heating-cooling jacket and vacuum pressure is frequently used to quickly evaporate solvent. Once the solution has reached the proper concentration which is determined by the density of the mother liquor (1.3594 - 1.3614 g/cm3 at 70 ºC), a constant vacuum pressure is held at 76.20 kPa for 30 - 40 min; the agitation rate is usually set to 250 rpm. In the first minute of process, the crystal seed is introduced. After 30-40 min of process (76.20 kPa of constant vacuum pressure), the vacuum pressure is increased up to 84.66 kPa following a predefined natural cooling trajectory. Sampling is performed at each 15 min of the process to obtain information from the experimental concentration (slurry) and CSD (Bolaños *et al*., 2008; Bolaños *et al*., 2014).

The methodology to perform this activity is as follows:

1. The Sampler Device (SD) is introduced vertically into the batch (see Figure 1) to obtain 10 mL of slurry (crystals and solution) without breaking the equipment's vacuum pressure.

2. A separation is performed to the sample through filtration to obtain a solution free of crystals. Density of the sample is measured in a high resolution digital densimeter Anton Paar® DMA 4500 (see Table 1 for a detailed description). The crystals obtained from the filtration process are used to measure CSD by using an imaging analysis. The procedure to quantify CSD is described next.

2.2 *Images acquisition system and CSD calculation*

Vision Assistant 2015 (National Instruments, Inc.) was used to analyze the crystals obtained at every sampling point of the experimental runs, i.e., every 15 min. This image-based approach is an alternative to diffraction laser technique in measuring both length and area of particles (crystals) in a direct way through Vision Assistant's software. This technique consists of acquiring ten images using a high resolution camera with HDMI interface and 60 Hz crisscross, and handling the light beam from a microscope trinocular. The sample is transported from the crystallizer to the imaging acquisition system by means of a peristaltic pump running at 1,500 rpm, without crushing the crystals during the operation. The camera captures ten square images which are filtered to reduce lens noise, avoiding undesirable light variations and is achieved through the threshold technique that allows the specification of a single image in the gray scale.

Areas with high density of crystals are isolated to be manually analyzed, and black pixels (crystals) are counted. The black pixels are compared with specific standards to decide if the crystal is presented or not according to binary images (background) (Hanks, 1997). An average of 100 crystal's areas are measured for each CSD analysis. A Neubauer's camera was used to count the particles and determine a conversion factor through simple calibration (Bolaños *et al*., 2008; Bolaños *et al*., 2014), i.e., the conversion factor enables a direct relation from 1 pixel (one-pixel side) to 1.074 μm (length). In this work, a microscope with a 10x ocular lens, a 40x objective and a Neubauer's camera was used for the measurement and analysis of the particles.

CSD results from this image-based approach were validated against laser diffraction by Cordova (2004), considering the area shape factor of K_A=1.212, reported by Quintana-Hernández *et al*., (2005). In addition, the experimental data of this work were compared against the results calculated by Bolaños *et al*., (2008) and Bolaños *et al*., (2014) using the same image-based approach discussed previously to avoid inclusion of errors caused by differences in CSD quantification technique.

Table 2. Feeding conditions for first experimental stage

Exp.	Initial feed of solution (g)	Second feed of solution (g)	% of second feed	Total solution (g)
1	7,295.20	4,863.46	40	1,2158.67
2	8,511.07	3,647.60	30	1,2158.67

3 Methodology

3.1 The first experimental stage

The approach used in this work is the use of a fractional feeding strategy of cane sugar solution (saturated) to feed the pilot-scale batch crystallizer, in order to deplete the dissolved solute in a greater proportion, because when the crystallizer is fed completely at the beginning of the process, crystals begin growing until a specific size, where sedimentation occurs at the bottom of the crystallizer if proper hydrodynamic conditions are not satisfied (Sander *et al*., 2012; Bolaños *et al*., 2014), which causes that lots of crystals do not participate in the mass transfer (dissolved cane sugar) to their faces (growth), resulting in a lower average diameter D(4,3), besides of high dispersion S(4,3). The benefit obtained by introducing a second charge to the crystallizer is that it promotes an increase in the growth rate to achieve the thermodynamic equilibrium of the system, because the second feed of saturated solution decreases the density of crystals per unit volume avoiding the presence of nuclei, generating a concentration gradient. This approach also seeks to resemble the operation strategy in the sugar industry, ensuring that the results derived from this work (pilot-scale plant) are applicable to industrial level.

The methodology carried out to determine the optimal amount (%) of the first feed (beginning of process) and second feed (after total evaporation time) that promotes further growth of the D(4,3) and FCM is described below.

This stage consists of 2 experiments performed twice, where both experiments were carried out under the following operating conditions, based on the results reported by Bolaños *et al*., (2008):

- Total evaporation time of 30 min with 72.80 kPa of vacuum pressure (63 °C)
- Solution concentration for both feeds: 1.3594 g/cm^3 at 70 ºC (commercial sugar and distillated water)
- Natural cooling temperature profile (adiabatic cooling (63 to 41 °C) forcing a change in the vacuum pressure from 72.8 to 84.60 kPa)
- Total process time of 90 min (total evaporation time and cooling)
- Constant agitation rate of 250 rpm

The first experiment began with the crystallizer filled up to 70% with saturated solution free of crystals, after the total evaporation time, the second feed (30%) was conducted to reach 100% of total crystallizer capacity (12,158.67 g). For the second experiment, the process began with the crystallizer filled up to 60% and then with the remaining 40%. Table 2 presents the detailed conditions of this experimental stage. The temperature of the second feed is specified according with the equilibrium temperature presented in the crystallizer, for 72.80 kPa (E1, E2 and E5) T = 64.50 ºC, for 76.20 kPa corresponds T = 60 ºC. Quantification of the CSD was carried out using the Images Acquisition System and CSD Calculation outlined above (Section 2.1). It is noteworthy to mention that sampling was not conducted in a defined range, since only the CSD and FCM were quantified at the end of process time (t_f = 90 min).

3.2 Second experimental stage

According to the results from the first experimental stage, discussed in the Results section, the conditions for the fractional feeding strategy that increase the total production of FCM_{t_f} and $D(4,3)_{t_f}$, and decrease $S(4,3)_{t_f}$, were identified. Subsequently, it was carried out a factorial experimental design (see Table 3), being the vacuum pressure and the total time of evaporation the two factors considered under study with 2 levels, obtaining a total of 4 experiments (E1 - E4) plus 4 replicates to ensure the degrees of freedom in the statistical analysis, sampling was realized every 15 minutes to arise the process final time of 90 minutes, each sampling point had ten images in order to obtain the CSD).

Table 3. Factorial experimental design

Exp.	Vacuum pressure	Total evaporation time
E1	72.80 kPa	30 min
E2	72.80 kPa	40 min
E3	76.20 kPa	30 min
E4	76.20 kPa	40 min

The vacuum pressure and the total evaporation time (which is related to the flow rate of steam into jacket) were selected as the two variables to be manipulated, this because the vacuum pressure regardless of its value will decrease the boiling point of the solution simplifying the evaporation of solvent (water) at low temperatures, avoiding degradation of the solute by thermal effects. To evaporate a greater amount of water, is it necessary to raise the temperature of the solution in a range of 2 to 3 °C over the equilibrium temperature; to fulfill this issue, it is required a proper handling of the steam flow rate into the heating jacket to avoid excessive evaporation, which was made possible by installing a proportional valve (Table 1). It was also decided to take in consideration the total evaporation time because it will be the period during which there will be the total evaporation of solvent (water) and is directly related to the required steam into the heating jacket, allowing to elevate the solution temperature, breaking the balance with the vacuum pressure.

This experimental design was proposed to achieve the goal of this article to analyze the effect of these two key variables on the trajectory described by the concentration process on the MSZW, which allows identification of an optimal concentration trajectory (supersaturation within the metaestable zone), to maximize FCM_{t_f} and $D(4,3)_{t_f}$, and minimize $S(4,3)_{t_f}$. The concentration of the process was determined by the density (g/cm^3) of the solution, measured in an Anton Paar® DMA 4500, while the response variables were determined separately as discussed in the Experimental Section. All measurements were performed every 15 min, generating a total of 7 measurements per experiment.

The density vs temperature curves used in this article to describe the MSZW (Figure 1) in the cane sugar batch crystallization from aqueous solution were the reported by Velázquez *et al.*, (2010) and are presented in eqs. 1 - 3. The term ρ_S represents the saturation curve, ρ_G the limit for the growth curve and ρ_N the limit for the nucleation curve. The valid operating range of these mathematical expressions is 40 ºC to 70 ºC, which is properly the range used for the experiments made in this article.

$$\rho_S = 1.28522 + 0.0014 \cdot T - 5.7875e-06 \cdot T^2 \quad (1)$$

$$\rho_G = 1.323293 + 5.397512e-04 \cdot T + 8.32078e-08 \cdot T^2 \quad (2)$$

$$\rho_N = 1.32254 + 8.325854e-04 \cdot T - 3.700576e-06 \cdot T^2 \quad (3)$$

Three experiments, were also conducted for performance comparison purposes: E5) vacuum pressure = 72.80 kPa and total evaporation time = 30 min, excluding fractional feeding strategy (the crystallizer is filled up to 100% capacity since the beginning), whereby it is possible to quantify the real profit produced by the strategy proposed in this work compared to previously reported operating conditions at pilot-scale plant (Bolaños *et al.*, 2008), E6) using the following operating conditions: vacuum pressure = 60.90 kPa, total evaporation time = 40 min, cooling temperature-trajectory = linearly from 70 ºC to 40 ºC (from 40 min to 90 min of process), including the fractional feeding strategy; these conditions are applied in a cane sugar industry, the scale-down from industrial conditions to Pilot Plant scale was carried out with the objective of emulate the industrial conditions at the pilot plant used in this paper and analyzing the feasibility that the new results obtained could be applied appropriately to industrial scale again, without affecting the operability of the industrial plant. This work seeks to evaluate the fractional feeding strategy proposed on a pilot plant scale using industrial operating conditions. This explanation was added to the manuscript at the end of section 3.2 Second Experimental Stage. Finally, experiment E7 is intended to apply the best strategy from the factorial experimental design, to quantify the benefit obtained using the strategy proposed in this work to the cane sugar industrial crystallization.

3.2.1 Vacuum pressure control

For regulation the vacuum pressure in the experiments performed into a pilot-scale batch crystallizer, a natural cooling-trajectory was applied, which reaches 84.60 kPa after the total evaporation time. For controlling the vacuum pressure, it was implemented a PI controller (k_p =4.10 and k_i =0.07 s^{-1}) using a proportional valve which regulates the access of air flow into the pilot-scale batch crystallizer (see Table 1 for more details), which helps to compensate the displacement of evaporated solvent (water) outside the pilot-scale batch crystallizer by effect of the vacuum pump.

In the experiment from the cane sugar industry (E6), the cooling temperature-trajectory generated by the vacuum pressure in an industrial-scale batch crystallizer to obtain the product was analyzed. It was observed that a linear profile of vacuum pressure after total evaporation time of 40 min with 60.90 kPa is followed. Then, eq. 4 was generated, which describes the vacuum pressure (kPa) along process time (min), imposed in industrial-scale batch crystallizer.

$$VP_{E6} = 60.90 + 0.2633 \cdot t \quad (4)$$

where VP_{E6} is the vacuum pressure for the experiment E6 and t is the process time expressed in seconds. Note that the units of eq. 4 are kPa for constant value, and kPa/min for the time coefficient.

3.2.2 Crystal seeds

The crystal seeds were obtained from commercial cane sugar with high purity (D(4,3)=450.00-550.00 ?m), which was crushed and then classified using sieves of size 150.00 μm, 180.00 μm and 212.00 μm. Crystals retained in the sieve of 180 μm were selected. In addition, it is worth mentioning that the sieve of 212.00 μm was used on top to limit the size range (S(4,3)) of particles in the sieve of 180 μm. Characterization (described in Section 2.1) of the crystal seeds obtained was performed, calculating a $D(4,3)_{seed}$=192.20 μm and $S(4,3)_{seed}$=11.20 μm.

Seeding is carried out inside the crystallizer extracting 100 ml saturated at 70 ° C, density 1.3594 g/cm^3 in a 250 ml vessel using a peristaltic pump (see Table 1) Subsequently, an amount of 3 g of seed is added into the vessel and homogenized with glass stirrer, avoiding agglomerations. After closing the crystallizer and with a time of 1 min, the existing slurry in the vessel (formed by 100 ml of saturated solution and the seed crystal) is introduced into the pilot-scale batch crystallizer through a small tube placed next to the crystallizer, the actual vacuum pressure within the system drives the slurry out of the vessel. Table 4 presents a summary of operating conditions for all experiments.

3.3 Crystallization kinetics

3.3.1 Nucleation rate

To fully understand the crystallization, it is necessary to know what happens at the microscopic scale of the process, which involves understating nucleation, crystal growth, breakage and agglomeration rates (Gerstlauer *et al*., 2002). The nucleation rate determines the amount of new particles generated within the continuous phase (solvent) when the concentration is located in a high supersaturation. It is classified into primary and secondary nucleation.

Table 4. Operating conditions for experiments E1 - E6

Property	**E1-E4**	**E5**	**E6**
Initial concentration	1.3594 g/cm^3		
Initial temperature	70 °C		
Initial sugar cane feed	6464.92 g	9235.60 g	
Initial water feed	2046.03 ml	2922.90 ml	
Second sugar cane feed	2770.68 g	----------	
Second water feed	876.87 ml	----------	
Constant vacuum pressure	72.80 kPa or 76.20 kPa	72.80 kPa	60.90 kPa
Total evaporation time (t_{vap})	30 min ó 40 min	30 min	40 min
Cooling temperature-trajectory	Natural cooling trajectory: 84.6 kPa	Natural cooling trajectory: 84.6 kPa	Linear cooling trajectory: 60.90 kPa – 84.60 kPa
Total time process	90 min		
Agitation rate	225 rpm		
Seeding time	t = 1 min		
Seed mass	3 g		
Seed's CSD	D(4,3) = 192.21 µm, S(4,3) = 11.20 µm		

Primary nucleation is divided in homogeneous and heterogeneous, which represent a) the formation of particles due solely to the change in concentration and b) by the presence of foreign particles or impurities which serve as nuclei, respectively (Mersmann, 2001). This work considers the homogeneous primary nucleation, because the experiments in pilot plant and industrial scale employ solution with 99.9% of purity, corresponding to the refining area of the industrial sector. Due to evaporation, air bubbles are developing and provide a surface that promotes heterogeneous nucleation. However, the influence of air bubbles is neglected for this study due to their short presence in the solution during evaporation.

Agglomeration, attrition, and breakage phenomena (secondary nucleation) are undesirable in the cane sugar industrial process because they yield low mean crystal size (D(4,3)) and wide dispersion size (S(4,3)). These phenomena are well known to be presented in the crystallization operation with high agitation rate. However, in this work we seek to avoid these phenomena by manipulating the agitation rate over a specific size of crystal seed. The constant agitation rate of 250 rpm was reported by Bolaños *et al*., (2014) on previous results to similar operating conditions at pilot-scale plant, where agglomeration only was presented with an agitation rate lower than 100 rpm. In the other hand, attrition, and breakage phenomena due to contact with impeller or reactor walls was observed for an agitation rate higher than 500 - 600 rpm. Therefore, with the constant agitation rate of 250 rpm, the secondary nucleation is minimized in the operating range.

To mathematically model the homogeneous and nucleation rate, different approaches have been applied, including the type power law equations, which have been widely and successfully used to characterize the effect of temperature and agitation rate in cane sugar crystallization (Mesbah *et al*., 2010; Bolaños *et al*., 2014). Another approach is the thermodynamic nucleation framework (Gerstlauer *et al*., 2002), which is based on thermodynamic and physicochemical properties of the solution under study, hence its reliability is higher compared against type power law equations (Mersmann A., 2001), allowing the calculation of the nucleation rate for different operating conditions. Therefore, it is considered a rigorous framework for calculating the crystallization kinetics. Eq. (5) is the mathematical representation of the homogeneous primary nucleation from classical nucleation theory. The solution requires few specific properties of the solution (diffusivity, viscosity, density and temperature).

$$B_{hom} = 1.5 D_{AB} (C N_A)^{7/3} \sqrt{\frac{\gamma_{CL}}{kT}} \frac{1}{C_C \cdot N_A} \exp\left[-\frac{16}{3} \pi \left(\frac{\gamma_{CL}}{kT} \right)^3 \left(\frac{1}{C_C \cdot N_A} \right)^2 \frac{1}{\ln(S_r)^2} \right] \quad (5)$$

The properties for the sugar solution can be predicted from the mathematical expressions derived by Mersmann A., (2001):

$$D_{AB} = \frac{kT}{2\pi \eta_L d_m} \quad (6)$$

$$\gamma_{CL} = kTK(C_C N_A)^{2/3} \ln\left(\frac{C_C}{C^*} \right) \quad (7)$$

$$S_r = \frac{C}{C^*} \quad (8)$$

$$C_C = \frac{\rho_C}{MW} \quad (9)$$

where ρ_C=1.588 g/cm^3 and PM=342.29 g/mol, k=Boltzmann constant and K=0.414 (Mersmann *et al*., 2002). The remaining parameters are listed in the nomenclature section. The concentration of saturation C^* is calculated using eq. (1) in terms of density.

Finally, to calculate the viscosity, a mathematical model (eq. 10) was adjusted from experimental data (Swindells *et al*., 1958), obtaining good predictions with R^2=0.9960 in a range of 65 - 75 Brix and 40 - 80 ºC.

$$\ln(\eta_L) = p_1 + p_1 \ln\left(\frac{1}{T} \right)$$
$$\ln(p_1) = 0.9831 \cdot \exp(0.0145 \cdot w_D S) \quad (10)$$
$$\ln(p_2) = 0.0828 \cdot \exp(0.0358 \cdot w_D S)$$

Eq. (10) uses data in terms of Brix for w_{DS} (weight of dry substance), in order to establish this equation on density units, eq. (11) is commonly used for this purpose; where SG represents specific gravity:

$$SG = \frac{w_{DS}}{258.6 - \left(\frac{w_{DS}}{258.2} \right) 227.1} + 1 \quad (11)$$

3.3.2 Crystal growth rate

In this work, we have assumed that only the solute dissolved (cane sugar) is crystallized and the solution is completely free of impurities (99.90% of saccharose). This is supported by the fact that for all the experiments, cane sugar of high purity and distilled water was used. As it was discussed by Mersmann *et al*. (2002) the crystal growth rate $\left(\frac{dv}{dL} \right)$ can be controlled by:

- Heat transfer

- Bulk diffusion and/or
- Surface integration

Quintana-Hernández *et al*. (2008) conclude that cane sugar crystallization is dominated by the surface integration mechanism, hence the crystal growth rate equations used to predict and describe this crystallization kinetic should include the integration mechanism. To further support this assertion, the following expression should be tested:

$$\sigma < 2x10^{-4}\sqrt{\frac{C_C}{C^*}} \tag{12}$$

The process of surface integration (v_{int}) is complex, and can be described by three different mechanisms:

- BCF (Burton, Cabrera, Frank) mechanism

$$v_{BCF} = 2.25x10^{-3}v^2\frac{D_{AB}}{d_m}\frac{\left(\frac{C^*}{C_C}\right)^{4/3}}{\ln\left(\frac{C_C}{C^*}\right)}\sigma^2 \tag{13}$$

- B+S (Birth and Spread) mechanism

$$v_{B+S} = \left(\frac{2}{\pi}\right)^{1/3}\frac{D_{AB}}{d_m}\left(\frac{C^*}{C_C}\right)^{3/2}\sigma^{3/2}[\ln(1+\sigma)]^{1/6}$$
$$\exp\left\{-\frac{\frac{\pi}{3}\left[K\ln\left(\frac{C^*}{C_C}\right)\right]^2}{v\ln(1+\sigma)}\right\} \tag{14}$$

- PN (Poly-Nuclear) mechanism

$$v_{PN} = \frac{D_{AB}}{3d_m}\left(\frac{C^*}{C_C}\right)^{2/3}\sigma^{3/2}\exp\left\{-\frac{\pi\left[K\ln\left(\frac{C^*}{C_C}\right)\right]^2}{v\ln(1+\sigma)}\right\} \tag{15}$$

In general, the crystal growth rate controlled by surface integration can be predicted by the three contributions:

$$v_{int} = v_{BCF} + v_{B+S} + v_{PN} \tag{16}$$

The set of equations (5) - (11) for primary nucleation and (12) - (16) for crystal growth rate were solved in JuliaLang 0.5.1 (Bezanson *et al*., 2015) using the experimental temperature and concentration acquired directly from the pilot-scale plant, to predict the crystallization kinetic rates at each sampling time. Also, prediction of crystal growth rate requires the knowledge of the crystal size, which was calculated using the image-based approach presented in 2.2 Images Acquisition System and CSD Calculation. This information allows to gain a full understanding of the microscopic level of the phenomenological effect of both considered factors: vacuum pressure and total evaporation time, on the key process states of primary nucleation and crystal growth rate.

4 Results

4.1 First experimental stage

This experimental stage served as a basis for determining the conditions of the fractional feeding strategy, to have a greater similarity to the operating conditions employed industrially, allowing exhaust the concentration of the saturated solution. The results of two experiments are shown in Table 5.

It is noted that for experiments with 60% and 70% of initial feed, FCM_{t_f} production significantly vary (1.4%). This result allows to define that there is an effect on production of FCM_{t_f} with the variation in % of feedings. This result had been expected as the FCM_{t_f} represents the yield, although both processes must reach the thermodynamic equilibrium ($S_r \rightarrow 0$) after a considerable process time (slow process due to crystallization dominated by surface integration), the second experiment is close to reaching the thermodynamic equilibrium at 90 minutes, while the first experiment is still far from it.

At industrial crystallization process, it is desired to increase the $D(4,3)_{t_f}$ without decreasing the FCM_{t_f}, being a target specification. However, according to the results reported by Bolaños *et al*., (2008) 4,865.10 g is obtained using the same operating conditions without the novel strategy of fractional feeding. This can be explained as the process did not reach the thermodynamic equilibrium and the end of process, where supersaturation was still presented ($S_r > 0$). Therefore, in this article an increase of 3.80% is obtained, compared linearly to industrial scale crystallizer with 35,000 kg capacity, this represents an increase of 316 kg. In addition, Velázquez *et al*., (2008) and Velázquez *et al*., (2010) report 3,900 g of FCM_{t_f} for the same operating conditions but with the seeding in the first 4 min of process. It is important to note that the amount of seed used is not reported, but from the results (supersaturation data), it is assumed that the seed quantity is lower than that used in this work (3 g) due to the low production of FCM_{t_f}.

Table 5. Results for feeding conditions

Exp.	Initial feed (%)	FCM_{t_f} (g)	$D(4,3)_{t_f}$ (µm)	$S(4,3)_{t_f}$ (µm)
1	60	4980.02	808.60	108.28
2	70	5050.14	944.64	143.81

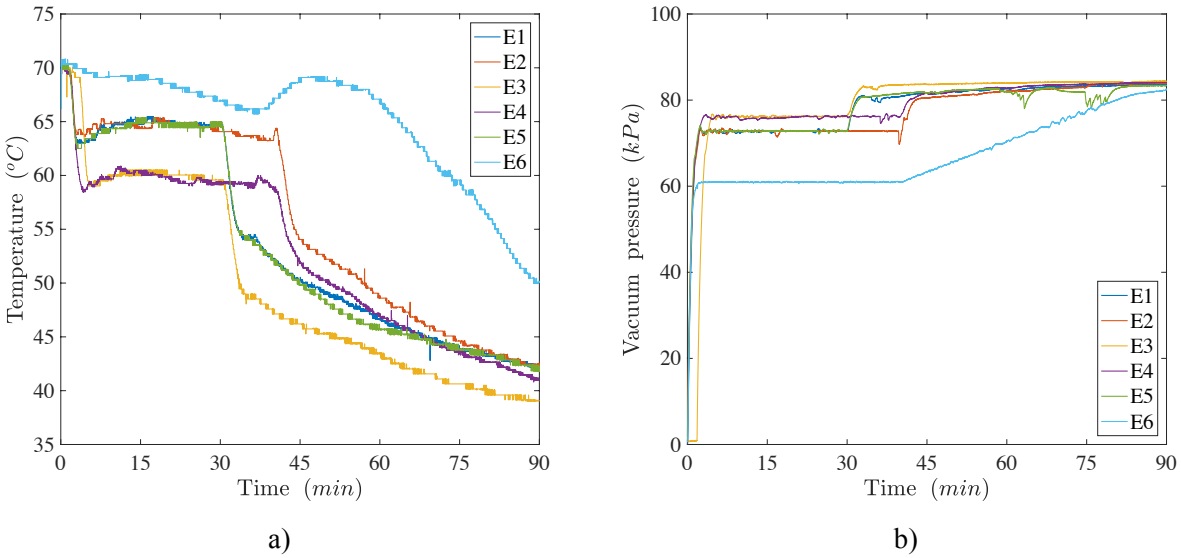

a) b)

Fig. 2. a) Experimental temperature and b) vacuum pressure.

Comparing these results, it can be seen that the amount of seed and time of introduction to the crystallizer significantly affect the production of FCM_{t_f}, since if the seed is not introduced into the crystallizer at the beginning of the process, e.g., t ≤ 1 min, high supersaturation is reached, creating the conditions for the concentration to be located within the nucleation zone in the MSZW, promoting competition for the available solute between the new nuclei with size L_0 and the crystal seeds ($D(4,3)_{seed}$=192.20 μm) and the marked decrease in FCM_{t_f} value. Therefore, the approach of fractional feedings represents an appropriate strategy to pilot-scale and industrial-scale operation, increasing the economic benefit from the best exhaustion of solute.

With regards to CSD, the $D(4,3)_{t_f}$ presents a significant variation, with a value of 808.60 μm and 944.64 μm for the experiments with 60 and 70% of initial feed, respectively. These results are due to the following: when 70% of initial feed is used, the particle density (n(L,t)) and the moments of the distribution of seed crystals are lower compared to the case of 60% of initial feed. This situation promotes high crystal growth rate due to the availability of solute, generating greater $D(4,3)_{t_f}$. Per those results, it can be expected that when 100% of initial feed is used, higher values of $D(4,3)_{t_f}$ will be obtained, however this is incorrect as supersaturation will be exhausted quickly ($S_r \rightarrow 0$) and there will be solute available to the end of the process avoiding the crystals grow.

Therefore, the experimental data for $D(4,3)_{t_f}$ represents a significant difference of 16.82%. Furthermore, the $D(4,3)_{t_f}$ values are higher than those obtained by Bolaños *et al.*, (2008) with $D(4,3)_{t_f}$ =732.72 μm , operating the crystallizer without the fractional feeding strategy. Again, the strategy proposed in this paper can make a profit of 28.9% for $D(4,3)_{t_f}$. A particular case is presented in Bolaños *et al.*, (2014) where they obtain a $D(4,3)_{t_f}$=1116.67 μm with the dynamic manipulation of the agitation rate with a range of 50-600 rpm and same operating conditions as well as the seed quantity. However, such strategy has some disadvantages: a) it is extremely complex to implement industrially, because the concentration of the mixture of sugar crystals and depleted solution is inferred offline[47] and b) using a high agitation rate (rpm> 450) modifies the natural crystal shape, eliminating the edges due to impacts

generated by the intense mixing (Kim *et al*., 2002), in addition to promoting secondary nucleation by crystal-impeller contact (Madras *et al*., 2007). Therefore, this strategy is not feasible to implement, because it has disadvantages compared with the novel strategy proposed in this paper.

Because of the observations described above, it was decided to perform the experiments in the second experimental stage with a fractional feeding of 70% at the beginning, and 30% after total evaporation time, to analyze the effect of the concentration process on CSD, FCM_{t_f} and MSZW.

4.2 Second experimental stage

4.2.1 Effects on crystal size distribution (CSD)

Figure 2 provides the temperature and vacuum pressure profiles for E1 - E6 experiments to see the complexity of events happening in the run. The temperature profile (Figure 2a) for each experiment is well described according with the trajectory desired. Also, the vacuum pressure is well controlled with the PI controlled described in Section 3.2.1.

The results obtained in this stage for experiments E1 - E6, with sampling time of 15 minutes are presented in Table 6 and plotted in Figure 3. The dynamic evolution of D(4,3) is described in Figure 3a, and the CSD in Figure 3c, where the remarkable similarity between experiments E1 - E4 can be appreciated (operating conditions from pilot-scale plant), obtaining a $D(4,3)_{t_f}$ of 925.92 μm, 1,035.19 μm, 995.49 μm and 1,089.45 μm, respectively. Those experimental data are mean values calculated from two replications. It is noted that the total evaporation time of 40 min (E2 and E4) promotes the increase for $D(4,3)_{t_f}$, however, for experiment E3, the dynamic evolution of D(4,3) is similar, declining its growth only towards the end of the process (t = 90 min), this is due to the use of a high vacuum pressure (76.20 kPa) which promotes solvent evaporation during the total evaporation time, by increasing the mass transfer from the dissolved solute to the seed crystals. For the experiment E1, where low levels of factorial experimental design were used, the $D(4,3)_{t_f}$ is lower with 10.55% against E2 and 12.60% against E4.

For the E5 results (experiment without fractional feeding, pilot-scale plant), it can be seen that early in the process, in the time range of 0 - 30 min, the D(4,3) has the same growth trend compared to E1 - E4, however, after the total evaporation time, there is a significant decrease in growth due to the absence of a second charge that decreases the density of crystals per volume of solution, therefore it gets a $D(4,3)_{t_f}$=672.89 μm, that is 38% lower against E4 (best result). In the case of experiment E6, which resembles the operating conditions of the cane sugar industry, it obtains a $D(4,3)_{t_f}$=338.07 μm. For this experiment, evaporation rate of the solvent in the first 30 min of process is low, so that mass transfer to the faces of the seed crystals is slow. Further, the cooling temperature-trajectory used is linear, that is, the cooling rate is lower compared with E1- E5 (natural cooling temperature-trajectory), equally causing a small $D(4,3)_{t_f}$. To achieve higher size of $D(4,3)_{t_f}$, the process time should be extended, increasing energy consumption. Figure 4 shows representative images of the crystals formed at the end process time (t_f =90 min), it includes experiments E1 - E6.

Analyzing Figure 3c, where CSD is plotted assuming a log-norm distribution (based on D(4,3) and S(4,3) from the image analysis), in a range from 0 μm to 1,200 μm, it is clear that the experiment E4 has the highest mean value for $D(4,3)_{t_f}$, compared to the remaining experiments. Another key characteristic is the % volume, where the highest values are desired to satisfy the target of a narrow CSD (low $S(4,3)_{t_f}$), hence experiment E4 again results with 42.48% volume, being the highest value from experiments E1 - E5.

To adequately quantify the effect on $D(4,3)_{t_f}$ for the considered factors, an ANOVA analysis was conducted using the data reported in Table 6, where it was found that the effect of the total evaporation time is significant with p=0.0422 for the increase of $D(4,3)_{t_f}$. In the opposite way, the vacuum pressure turned out to be not significant with p=0.1184 (significant if p<0.05), which is opposed to that observed experimentally. This result is attributable to the fact that the levels of the vacuum pressure were similar, so its effect is minimum and there may be not significant difference between the mean values.

For the case of S(4,3) (see Figure 3b), ANOVA applied to the experimental design reveals that the vacuum pressure (p = 0.7723) and total evaporation time (p = 0.4649) are not significant (significant if p<0.05), hence the S(4,3) does not present a clear trend for the factors considered in the analysis. Also, the increase in S(4,3) is directly related to the increase of D(4,3). This phenomenon can be observed for E6, where the $D(4,3)_{t_f}$ is 338.07 μm, and consequently, the $S(4,3)_{t_f}$ obtained is 52.02 μm, lower compared with E1 - E5. Variable behavior presented in Figure 3b will be explained in the Analysis of effects on slurry concentration Section.

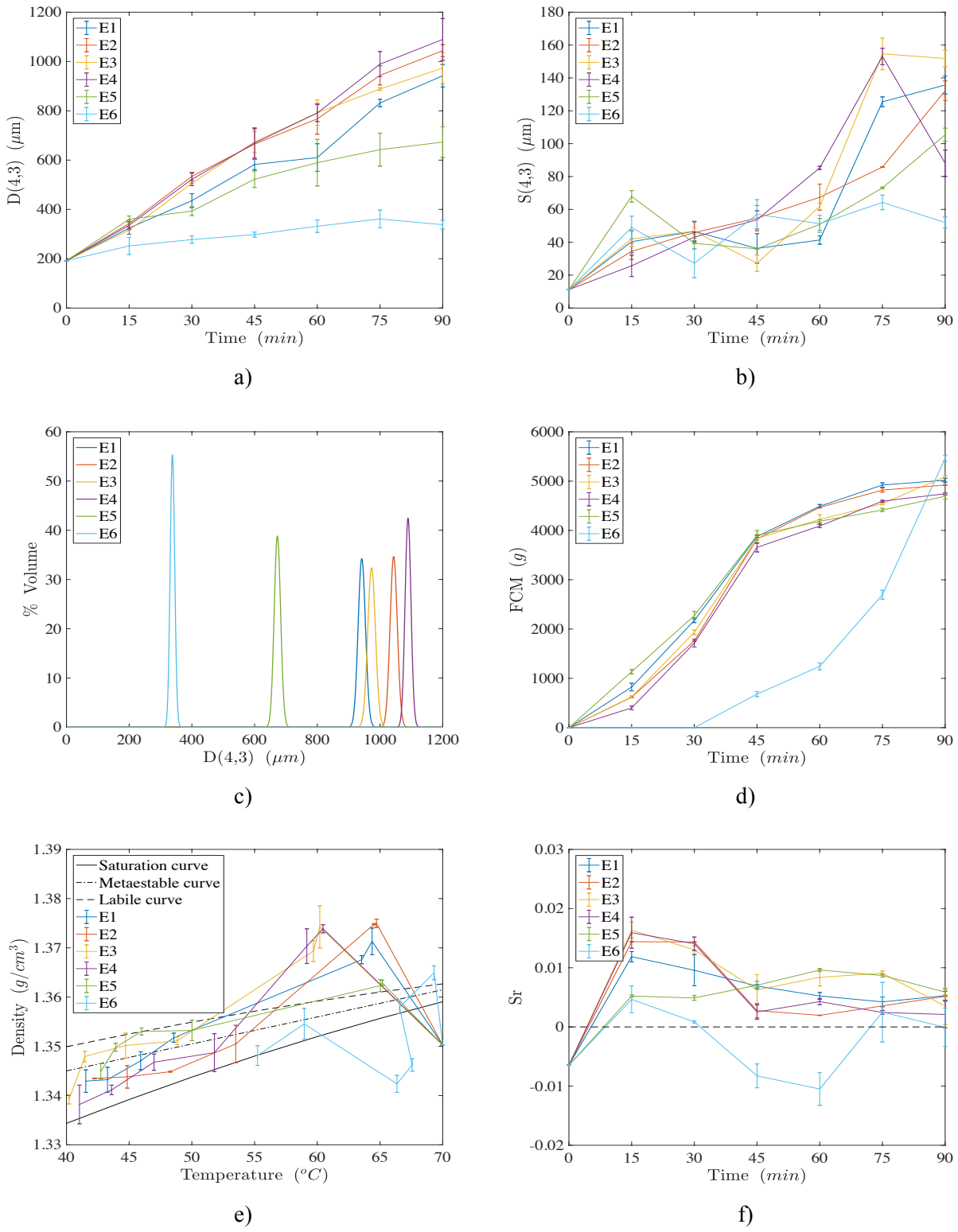

Fig. 3. Experimental results: a) D(4,3), b) S(4,3), c) CSD_{tf}, d) FCM, e) MSZW and f) Sr.

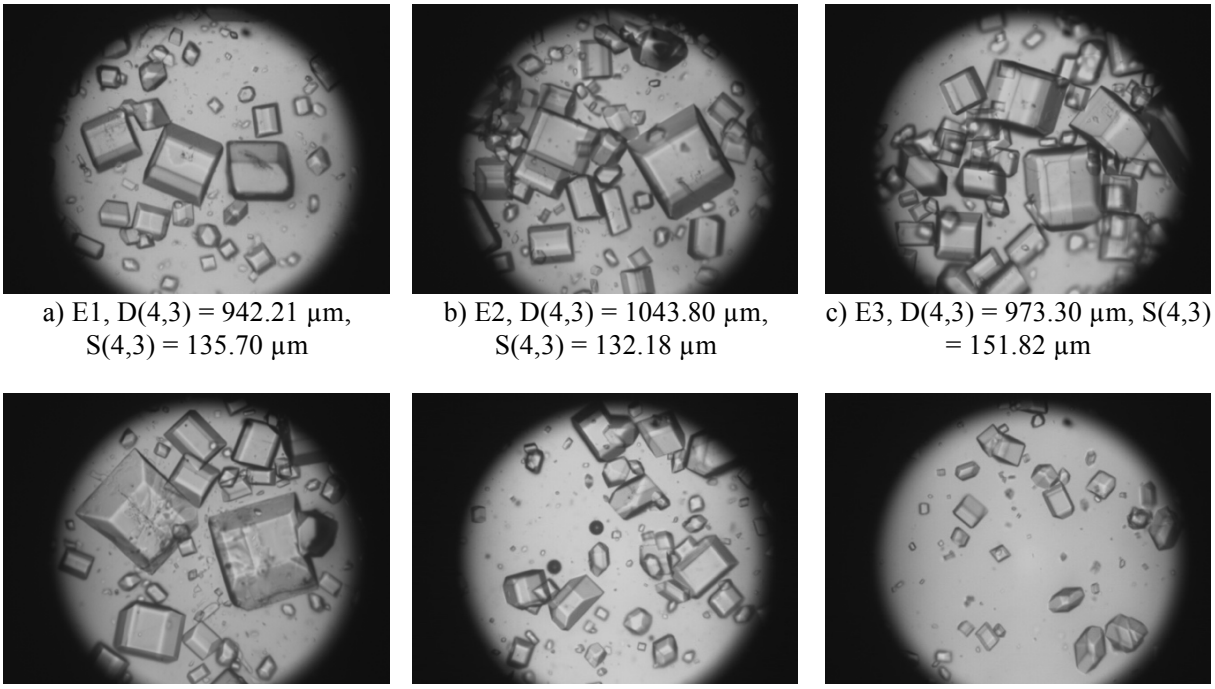

a) E1, D(4,3) = 942.21 µm, S(4,3) = 135.70 µm
b) E2, D(4,3) = 1043.80 µm, S(4,3) = 132.18 µm
c) E3, D(4,3) = 973.30 µm, S(4,3) = 151.82 µm
d) E4, D(4,3) = 1089.50 µm, S(4,3) = 88.10 µm
e) E5, D(4,3) = 672.89 µm, S(4,3) = 101.41 µm
f) E6, D(4,3) = 338.07 µm, S(4,3) = 52.02 µm

Fig. 4. Representative images for cane sugar crystal for the experiments: a) E1, b) E2, c) E3, d) E4, e) E5 and f) E6.

Table 6. CSD and FCM experimental data at final time.

Experiments	Key process variable		
	$D(4,3)_{t_f}$, µm	$S(4,3)_{t_f}$, µm	FCM_{t_f}, g
E1	974.39 909.77	135.70 131.82	5018.78 4991.28
E2	1060.95 1026.61	132.18 106.36	4921.01 4919.96
E3	928.92 1017.69	151.82 176.95	5091.58 5205.64
E4	1149.49 1029.54	88.10 136.19	4744.13 4657.83
E5	759.51 586.28	105.41 115.90	4694.37 4653.11
E6	350.70 325.56	52.02 28.41	5463.81 5762.30

4.2.2 Effects on FCM

The FCM is the yield of the process and depend on the different operating conditions applied, which carry out to reach the thermodynamic endpoint at infinite time (Sr). Nevertheless, in the cane sugar industrial crystallization its phenomenological behavior has rarely been studied, since most research has focused about the manipulation of the CSD. In this context, some authors have reported that FCM is not significantly affected by the variables involved in the crystallization, e.g., agitation rate, impeller geometry or temperature (Akrap *et al*., 2010; Kaćunić *et al*., 2013; Bolaños *et al*., 2014). However, it is known that cane sugar crystallization has low mass transfer due to surface integration mechanism, producing different concentration gradients even at the same temperature. For this situation, at the final process time (90 min) (feasible process time), we have different yields of

FCM and depend strongly on the thermodynamic endpoint in this process time, which is not always reached due to the different operating conditions applied (Table 3 and 4).

The results for the FCM are presented in Figure 3d and Table 6. As discussed above in the first experimental stage (Section 4.1), the FCM_{t_f} presents slight variations with respect to the amount (%) of feed charge and changes in operating conditions in the vacuum pressure and total evaporation time. Thus, the ANOVA analysis is consistent obtaining p = 0.7486 for vacuum pressure and p = 0.6793 for total evaporation time. On average for experiments E1 - E5, FCM_{t_f}=4,894 g is obtained. In the case of experiment E6 (operating conditions at cane sugar industry), the FCM was scaled (using a volume relation V_{ind}/V_{PP}) to allow a comparison with the results from experiments E1 - E5 (operating conditions for pilot-scale plant). The FCM dynamic evolution from experiments E6 is opposed to experiments E1- E5, producing no crystallized mass in the first sampling point (t=15 min). Later, the production of FCM at total evaporation time (t=40 min), it increased suddenly to reach final process time (t_f=90 min). Then, experiment E6 produced higher FCM_{t_f} of 5,613.06 gr (t_f=90 min) due to the complete depletion of Sr (see Figure 3f for experiment E6). However, the $D(4,3)_{t_f}$ is small (338 μm) due to that concentration process got out the saturated zone causing the dissolution of crystals. This phenomenon is discussed in Section 4.2.3.

On the other hand, the amount of evaporated water (EW) was quantified by displacement effects of steam from inside the crystallizer due to the heat supplied from the jacket. The knowledge of the dynamic behavior of solvent evaporation is important since it allows to quantify the change in volume of the continuous phase (solution), needed to complete the mass, energy and population balances for modelling purposes. The experimental data were fitted by least squares using JuliaLang 0.5.1 (Bezanson *et al*., 2015), obtaining the following expression:

$$EW = 1037 - 36.18 \cdot t - 3.502 \cdot t_{vap} - 0.5213 \cdot t^2 - 2.818e-03 \cdot t \cdot t_{vap} - 2.706e-03 \cdot t^3 + 4.224e-04 \cdot t^2 \cdot t_{vap} \quad R^2 = 0.9343 \qquad (17)$$

The adjusted mathematical empirical model is time-dependent and includes the total evaporation time (t_{vap}), it predicts the amount of water evaporated for the specific conditions employed in the set of experiment E1 - E4 (see Table 4).

Usually, in industrial applications there are a considerable number of unknowns, which hamper the use of pure theoretical considerations in the dynamic modelling for the crystallizer's volume. To overcome this situation, some empirical models have been developed based on the boiling point elevation (BPE) and the solution saturation temperature (Georgieva *et al*., 2003) and in the worst case, constant linear evaporation rate is supposed (Choong and Smith, 2004). Georgieva *et al*., (2003) reports the more promising approach for modelling the dynamic volume, but it includes a constant parameter (k_{vap}) that must be estimate from experimental data. Hence, eq. (17) represents an efficient alternative to compute the amount of evaporated water dynamically in cane sugar batch crystallization, without any previous estimation for unknown parameters.

4.2.3 Analysis of effects on slurry concentration within MSZW

Figure 3e is a diagram of concentration (density) vs temperature for the crystallization zones (MSZW), where metastable curve represents the limit of the growth zone and the labile curve correspond to the limit of the nucleation zone (Quintana-Hernández *et al*., 2016). This diagram shows the density routes for each experiment against MSZW (eqs. 1 - 3), where special attention was held to begin each experiment with the proper saturation density ρ_{sat}=1.3594 g/cm^3 at 70 °C. Theoretically, when the process density is among the region delimited by the saturation curve and the metaestable curve, maximum production of FCM_{t_f} is given (Bolaños *et al*., 2008).

As can be seen, for experiments E1 - E4, the density begins close to the saturation curve with 70 ºC, later to increase dramatically to reach the nucleation zone in the first sampling time (t = 15 min), where nucleation occurs spontaneously and produces crystal with low purity. This experimental behavior occurs because the crystallizer has a low level of solution, combined with the evaporation of solvent (water) and the low mass transfer from solution to seed due to the surface integration growth mechanism, promoting a rapid increase in density. In this sampling time, a significant difference is presented in the equilibrium temperature due to vacuum pressure, where E1 and E2 achieve ρ_{E1}=1.3713 g/cm^3 and ρ_{E2}=1.3750 g/cm^3 with an equilibrium temperature of 64.50 ºC, E3 and E4 achieve ρ_{E3}=1.3743 g/cm^3 and ρ_{E4}=1.3739 g/cm^3, respectively, with an equilibrium temperature of 60 ºC, allowing an increase in solvent evaporation for

reduced boiling point, due to a higher pressure vacuum (76.20 kPa). Subsequently, in the second sampling time (t = 30 min), density decreases, but remains even within the nucleation zone. When the second charge is fed into the crystallizer (30 min for E1 - E3, 40 min for E2 - E4), the density decreases abruptly to locate the concentration within the nucleation zone or growth.

It is important to highlight the effect of the introduction of the second charge, which is to regulate the concentration of the process properly, carrying out the crystallization efficiently within the desired zones in the MSZW. At this point, the total evaporation time has a significant effect, since when is applied with 30 min (E1 & E3), the densities achieved (ρ_{E1}=1.3517 g/cm^3 and ρ_{E3}=1.3511 g/cm^3) are located within the nucleation zone, which it is also undesirable because it governs the kinetics of formation of new small nuclei, and reduce the growth of seed crystals. This behavior allows to predict that the $S(4,3)_{t_f}$ will be higher compared to that obtained for E2 and E4. This can be seen in Figure 3b, where E1 and E3 are the ones with the highest standard deviations in % volume with $S(4,3)_{t_f}$=135.70 μm and $S(4,3)_{t_f}$=151.82 μm, respectively. Towards the end of the process (t = 90 min), the four experiments are located and maintained in the growth zone, with experiment E4 ending closest to the saturation curve, where theoretically the best performance is obtained for $D(4,3)_{t_f}$, which agrees with that observed in Figure 3a and discussed in the Effects on CSD Section.

In the case of the comparative experiment E5, it is noted that the increase in density at the first sampling time (t = 15 min) is less compared with E1 - E4, that is because the total charge in the crystallizer is performed early in the process (t = 0 min), hence solvent evaporation does not greatly affect the density. However, and as shown in Figure 3e, the density is established during 75 min of process within the nucleation zone, causing the crystal seeds do not grow as expected, obtaining a lower $D(4,3)_{t_f}$ (see Figure 3a). Moreover, in case for the FCM_{t_f} lowest result is obtained with 4694.40 g.

Finally, experiment E6 shows that the density has erratic behavior, reducing its density after the third sampling time (t = 45 min), reaching the unsaturated zone and then returning to the growth zone at 75 min. This causes the continuous phase (mother liquor) to acquire solute, due to dissolution of the seed crystals, inhibiting their growth, so a $D(4,3)_{t_f}$=338.07 μm is obtained. As discussed above, the technique used in the cane sugar industrial crystallization is not suitable because it produces crystals with a small $D(4,3)_{t_f}$, requiring an increase in processing time and repeated charges of mother liquor in the highest level of concentration (74º Brix) from the evaporation stage to reach the standard size of 450 μm (Chen C., 2000).

The strategy proposed in this work greatly improves the performance of cane sugar industrial crystallization, since the industrial target for D(4,3) (450.00-550.00 μm) is reached after 45 min of process, with a FCM = 4,000.00 g. This allows reducing the processing time by at least 50%, increasing the number of batches produced by each workday, and in terms of energy, reducing steam consumption in each batch, increasing overall performance.

Although supersaturation in terms of density is widely used in sugar industry, it would be useful to provide Table 7 with the relationship between density and concentration. This would aid crystallization enthusiasts from different fields and might held them refer to the results and conclusions of this work much easily.

Another way of representing the concentration trajectory is through supersaturation (S_r), where a value within the metastable zone is desired with a value close to zero at the end of process time, e.g., Sr≥0. The S_r diagram is presented in Figure 3e, where the S_r for all experiments suddenly increase to reach a maximum value at the first sampling time (15 min). Then, at the end of the process (t = 90 min) a complete depletion has not been reached, but the values are close to 0, with the exception of experiment E6 where the complete depletion of S_r was reached. Thus, this diagram is a simple and practical tool for identifying routes concentration process and predict the quality of the final product, as the case of the experiment E6, where a zone with negative values (unsaturated zone) for S_r is identified, which means that no crystallization occurs and no supersaturation, hence no driving force is presented. At the industry level, this diagram can be very useful because it allows a direct comparison between different operating strategies, facilitating the selection of the most appropriate, which meets specific quality requirements.

4.2.4 Effects on nucleation rate

The experimental data reported in Figure 3d (density and temperature) from experiments E1 - E6 were used for the solution of eqs. (5) - (11). Figure 5 shows the dynamic behavior of the nucleation rate. It can be seen that at the beginning of each experiment (t=0 min), the concentration of all experiments is close to solubility curve at 70 °C (see Figure 3d), hence nucleation

Table 7. Relationship between density and concentration at final time

Experiment	Density (g/cm^3)	Concentration (g/ml)
E1	1.3429	2.4542
E2	1.3434	2.4758
E3	1.3392	2.3624
E4	1.3381	2.3545
E5	1.3449	2.5130
E6	1.3480	2.8008

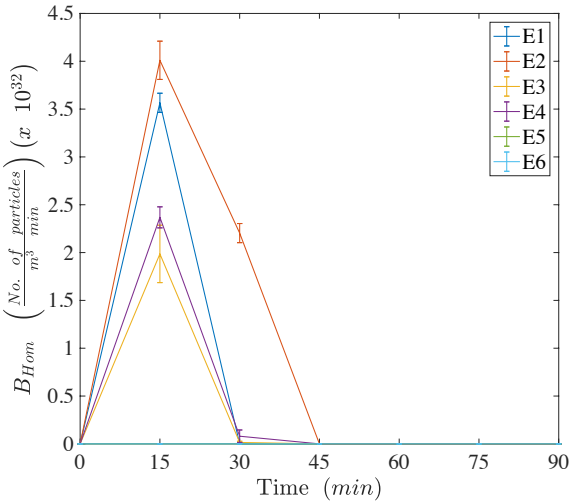

Fig. 5. Nucleation rate.

should not occur at this stage. Subsequently, at the first and second sampling time (15 min and 30 min), all experiments show a sudden increase the nucleation rate (Figure 5) because the process remains within the total evaporation time of solvent, causing an increase in the solute concentration per unit of solvent (ρ >1.3700 g/cm^3), while maintaining a constant temperature.

According to Quintana-Hernández *et al*., (2008) cane sugar crystallization is dominated by integration, being reflected in long crystallization times, hence increasing the concentration by effect of solvent evaporation, the system can not achieve the thermodynamic equilibrium quickly by migrating solute to the faces of the seeded crystals (slow-mass transfer). This microscopic behavior promotes the ideal conditions to achieve $\partial G/\partial L = 0$, allowing the primary homogeneous nucleation to occurs. Experiments E5 and E6 (industrial case) are the ones which show the minimum nucleation rate due to the operating conditions imposed.

The effect of vacuum pressure and temperature in experiments E1 - E4 is remarkable. When using a lower vacuum pressure of 72.80 kPa for E1 and E2, the temperature of the solution will be higher (64.50 ºC) during the total evaporation time (30 - 40 min, see Table 3 and 4), which generate higher nucleation rate (3.11×10^{29} (No. of particles)/(m^3· min)). For a higher vacuum pressure of 76.20 kPa for E3 and E4, the nucleation rate is lower (1.90×10^{29} (No. of particles)/(m^3· min)) due to the equilibrium temperature will be also lower (60 ºC), resulting in a lower nucleation rate than E1 and E2.

We can establish that the higher the temperature (64.50 °C), the rate of nucleation will also be high when supersaturation (S_r) is located above the growth zone (1.3549 g/cm^3). in this case, the nucleation is minimized by the effect of concentration at the third sampling time (45 min), which is within or close the growth zone (first metastable zone between 1.3437-1.3504 g/cm^3 at 50 °C). For experiments E5 and E6, the nucleation rate is not significantly appreciable due to the use of a linear cooling profile, which enables the concentration to be located close to the growth zone at all sampling times. This is supported by Figure 3b, where S(4,3)$_{t_f}$ is the lowest for E5 and E6.

The experiment E6 is a special case (industrial case), where the cooling-temperature trajectory steers the process to concentrations below the solubility curve, which favors the new crystals formed by nucleation to be dissolved, decreasing S(4,3) (see Figure 3b), but this also causes the D(4,3) of seeded crystals to decrease, as shown in Figure 3a. This behavior is undesirable in crystallization, as it makes the concentration fall in an unsaturated zone, to subsequently place it in a supersaturated zone again, which generates higher energy costs by recrystallization of dissolved solute. However, this problem can be solved through an adequate controlled strategy, carrying out an intermediate heating stage to cause fines dissolution, decreasing variability S(4,3) and improving the quality of the batch in terms of CSD (Myronchuk *et al*., 2013).

From the analysis of results made in this section, it can be defined that the operating strategy (see Table 4) for experiments E4 present the best results in terms of nucleation rate, avoiding excessive formation of new particles, allowing seed crystals have higher particle size D(4,3) (see Figure 3a), and represent a major improvement when applied at industrial cane sugar crystallization, which is discussed in Section 4.2.

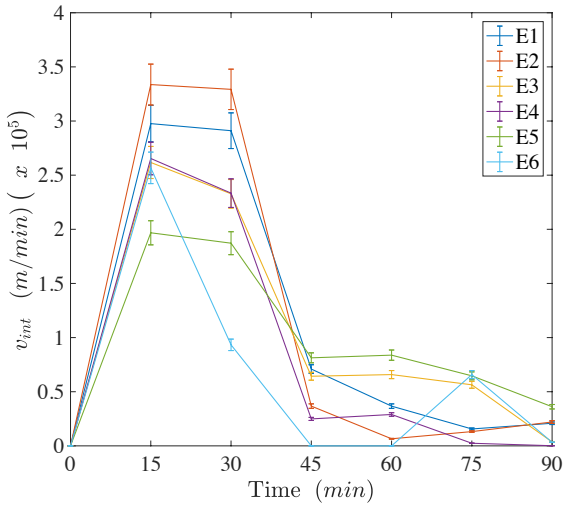

Fig. 6. Crystal growth rate.

4.2.5 *Effects on crystal growth rate*

The growth rate calculated by solving eq. (15) is presented in Figure 6, and has been studied reflecting similar behavior to the curve of supersaturation. (Bolaños, 2000) The effect of different operating conditions on the crystal growth rate in experiments E1 - E6 is clear, and two different behaviors can be identified. First, E1 - E2 and E5 have an average growth rate of 3.68×10^{-5} m/min at the first sampling point (t=15 min), while for experiments E3 and E4 an average of 3.01×10^{-5} m/min. This is attributed to differences in equilibrium temperature and the evaporation rate for each experiment during the total evaporation time (different vacuum pressure described in Table 3). Those factors cause faster crystal growth rate with high equilibrium temperature of 64.4 ºC, while a low equilibrium temperature of 60 ºC results in lower crystal growth rate.

For the experiment E6 (industrial case) the crystal growth rate is presented with 3.45×10^{-5} m/min, with a temperature of 69.29 ° C propitiated by the slow cooling gradient of temperature (see Table 4). For the second sampling time (t=30 min), it is expected that E1-E5 experiments maintain the same growth rate because the operating conditions remain unchanged. Subsequently, as supersaturation (S_r) is depleted (Figure 3e) by the process endpoint, the crystal growth rate decreases to near 0. From the above, it is identified that experiment E4 is depleting further S_r, which represents that the greater amount of dissolved solute was crystallized, increasing $D(4,3)_{t_f}$ and obtaining a crystal growth rate close to 0 at 90 min (end of process). This can be corroborated by analyzing Figure 3a, where E4 obtain $D(4,3)_{t_f}$=1089.50 μm.

The largest $D(4,3)_{t_f}$ produced by this experiment is explained even though the peak (t=15-30 min) was lower (3.04×10^{-5} m/min) compared to experiments E1 - E2. This experiment featured a lower nucleation rate (formation of new smaller particles), therefore the growth of the seeded crystals with D(4,3)=192.20 μm was favored compared to other experiments, where there was a competition for the solute between the seeded crystals and new crystals formed due to nucleation rate with characteristic size $L = 7.49 \times 10^{-9}$ m (Khaddour *et al.*, 2010).

Experiment E6 (industrial case) shows a highly undesirable behavior because, 45-60 min into the process, the concentration is in an undersaturated zone (negative values in Figure 3e), which favors a dissolution of the seeded crystals, and subsequently returns to the first metastable zone at the end of the process. This result is easily confirmed in Figures 3a (low $D(4,3)_{t_f}$), 3e (low density values), 3f (negative values), 5 (null nucleation rate) and 6 (null crystal growth rate) and this reflects the inadequate operation strategy which is currently used in the cane sugar industrial crystallization, so the implementation of the proposed strategy in this work represents a substantial improvement, allowing to increase the quality of cane sugar and lower energy costs to avoid dissolution and recrystallization.

4.3 *Validation at cane sugar industrial crystallization*

By the results discussed in previous sections, the operating strategy for experiment E4 (Table 4) was applied at industrial level, in order to analyze the real benefit of the proposed strategy compared to the current cane sugar industrial crystallization approach (experiment E6). This validation was done due to the industrial crystallizer has a capacity of 20,000 Kg, hence the results from experiment E4 may not be scale-up linearly, mainly due to the differences in the crystallization kinetics, and hydrodynamic regime of the crystallizer itself.

Figure 7a presents the comparison for the results from experiments E6 and E7. Values of E6 for FCM were scale-up to allow a direct comparison to the experiment at industrial level E7 by using the volume relation V_{ind}/V_{PP}. It is remarkable the differences in D(4,3), where E6 has a $D(4,3)_{t_f}$=338.07 μm, while E7 has $D(4,3)_{t_f}$=611.36 μm, which means that the proposed strategy allows increasing in 55.29% the $D(4,3)_{t_f}$ with respect to the current operation

approach. For the case of S(4,3), a significant increasing in S(4,3) is observed for experiment E7 compared to E6. This phenomenon is well known to be presented, as D(4,3) increase S(4,3) will increase too. This explanation can also be confirmed with experiment E6, where a low growth of D(4,3) was obtained, and therefore low S(4,3) is expected. As discussed previously, this result is lower due compared to experiment E4. However, the benefit is clear and the cane sugar industry can get substantial economic benefits through changes in operating conditions for the proposed in this paper.

CSD is plotted in figure 7c assuming a log-norm distribution (based on D(4,3) and S(4,3) from the image analysis), in a range from 0 μm to 1200 μm. It is clear that the experiment E7 improves the CSD due to the highest mean value for $D(4,3)_{t_f}$, compared to the E6 experiment. Lower value for % volume in experiment E7 are attributed to the high S(4,3) value reported in figure 7b.

Regarding FCM_{t_f}, figure 7d shows that at 90 min, E7 get FCM_{t_f}=15,881.11 g, while E6 after the scale-up get FCM_{t_f}=14,975.20 g, satisfying the target specification of getting the high FCM_{t_f} for the approach proposed and current strategy at the end of process.

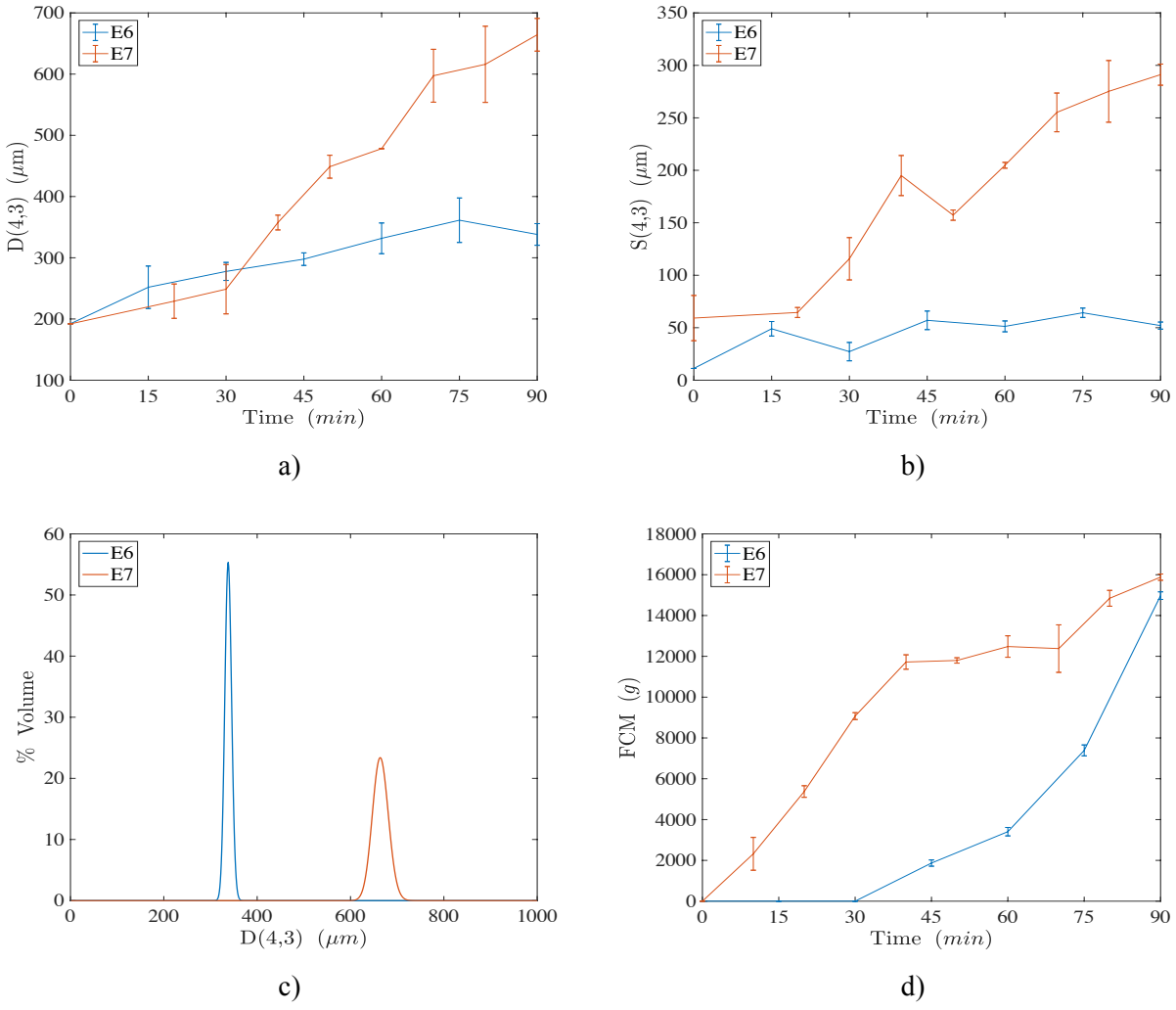

Fig. 7. Validation at industrial level: a) D(4,3), b) S(4,3), c) CSD_{tf} and d) FCM.

Conclusions

A study on the effects of vacuum pressure and total evaporation time on the concentration (density) in the MSZW for the batch crystallization of cane sugar was conducted. In addition, a novel approach of fractional feeding was proposed in order to improve the quality of the final product in terms of CSD and FCM. Seven experiments are reported (performed twice), where four of them followed a factorial experimental design to determine the effect of vacuum pressure and total evaporation time on $D(4,3)_{t_f}$, FCM_{t_f}, the MSZW and the crystallization kinetics. The fifth experiment was conducted to compare the profit obtained by the application of the proposed approach, the sixth to evaluate the current operating conditions from industrial level and the seventh to evaluate the real benefit of the proposed strategy in an industrial scale crystallizer. From the results, it is concluded that the more efficient strategy for the fractional feeding was: to begin the process with 70% of saturated solution of the total mass (12,158.67 gr) using water vapor for 40 min (total evaporation time) to obtain the massecuite (using 76.20 kPa of vacuum pressure). Then, 30% of saturated solution is fed to manipulate the concentration within the saturation and metastable curves from 40 to 90 min without using water vapor, reducing its consumption (using 86.60 kPa of vacuum pressure).

The effects of vacuum pressure and total evaporation time were not significant for FCM_{t_f}. The obtained results for $D(4,3)_{t_f}$ and FCM_{t_f} using the operation strategy presented in this work are better when compared to the operating conditions from industrial level. Therefore, it can be concluded that the current industrial strategy benefits only in FCM_{t_f} but not for $D(4,3)_{t_f}$, hence adjusting operation conditions would increase the yield and economic benefit of industrial cane sugar crystallization.

Relating these observations to MSZW, it can be concluded that:

- High vacuum pressure at the beginning of the process moves the concentration toward the labile zone, which promotes an increase in S(4,3). Subsequently the concentration returns to the nucleation or crystal growth zone by effects of natural cooling temperature-trajectory imposed. To avoid abrupt effect of vacuum pressure at startup, this strategy can be implemented gradually during the first 15 minutes of process, giving enough time for adequate mass transfer.

- The introduction of the second charge locates the concentration in the growth zone in the MSZW by decreasing the density of the solution, promoting an increase in crystal growth rate to generate faster depletion of Sr.

- Operating conditions from industrial crystallization are not adequate, as these push the concentration to an unsaturated zone, causing partial dissolution of the crystals formed, decreasing the average crystal size D(4,3) and increasing operating costs. These issues do not meet specifications required to obtain a high quality product.

Finally, the conclusions for the crystallization kinetics are:

- Vacuum pressure strongly affects nucleation and crystal growth rate. Higher vacuum pressure would lower both nucleation rate and growth rate and vice versa.

- With regards to seed crystals, the nucleation and crystal growth rate are closely linked, because increasing the nucleation rate, the crystal growth will also increase. It is preferred to avoid nucleation rate as D(4,3) will no increase as expected due to the competition between the formation of new particles (primary homogeneous nucleation) and growth on the seeded crystals (crystal growth).

- Analysis by images acquisitions (D(4,3) and S(4,3)) corroborates that the operation strategy for the cane sugar industrial crystallization with total evaporation time of 40 min with a vacuum pressure of 76.20 kPa, including the fractional feeding strategy, followed by a natural cooling-temperature trajectory is viable to employ at the industrial level, increasing the key process parameters $D(4,3)_{t_f}$ and FCM_{t_f}.

Nomenclature

B_{hom}	primary homogeneous nucleation rate, (No. of particles)/(m^3·s)
C	molar concentration, kmol/m^3
C*	saturation molar concentration, kmol/m^3
C_C	crystal molar concentration, kmol/m^3
d_m	molecule diameter, m
D(4,3)	average diameter in % volume, μm
D_{AB}	diffusion coefficient, m^2/s
dL	change in crystal length, m
dv	change in crystal growth rate, m/s
∂G	change in total enthalpy
EW	evaporated water, kg
FCM	formed crystal mass, kg
k	Boltzmann constant, 1.381×10^{-23} J/K
K	factor, dimensionless
MSZW	metastable zone width
MW	molecular weight, kmol
N_A	Avogadro's number, 6.023×10^{26} kmol^{-1}
S_r	supersaturation ratio, dimensionless
S(4,3)	standard deviation in % volume, μm
SG	specific gravity, dimensionless
t	time, min
t_f	final process time, min
T	absolute temperature, K
v	stoichiometric coefficient
v_{int}	crystal growth rate, m?s
VP	vacuum pressure, kPa
VP_{E6}	vacuum pressure for experiment E6, kPa
V_{ind}	industrial crystallizer volume, L
V_{PP}	pilot-scaled plant crystallizer volume, L
t_{vap}	total evaporation time, min
w_{DS}	weight of dry substance, g/100g

Greek symbols

η_L	dynamic viscosity, Pa·s
γ_{CL}	interfacial tension, J/m^2
σ	relative supersaturation, dimensionless
ρ_C	density of crystal, kg/m^3

References

Aamir, E., Nagy, Z. K., Rielly, C. D. (2010). Evaluation of the effect of seed preparation method on the product crystal size distribution for batch cooling crystallization processes. *Crystal Growth Design 1*, 4728-4740.

Akrap, M., Kuzmanic, N., Kardum, P. J. (2010). Effect of mixing on the crystal size distribution of borax decahydrate in batch cooling crystallizer. *Journal of Crystal Growth 312*, 3603-3608.

Bezanson, J., Edelman, A., Karpinski, S., Shah, V. B. (2015) Julia: A fresh approach to numerical computing. arXiv:1411.1607v4.

Binev, D., Seidel-Morgenstern, A., Lorenz, H. (2015). Study of crystal size distributions in a fluidized bed crystallizer. *Chemical Engineering Science 133*, 116-124.

Bolaños, R. E., Sánchez, S. K. B., Urrea, G. G. R., Ricardez, S. L. A. (2014). Dynamic modeling and optimization of batch crystallization of sugar cane under uncertainty. *Industrial and Engineering Chemistry Research 53*, 13180-13194.

Bolaños, R. E. (2000). Control and optimization of operating conditions from cooling batch crystallizers. Ph. D. Thesis. I.T. de Celaya, México.

Bolaños, R. E., Xaca, X. O., Álvarez, R. J., López, Z. L. (2008). Effect analysis from dynamic regulation of vacuum pressure in an adiabatic batch crystallizer using data and image acquisition. *Industrial and Engineering Chemistry Research 47*, 9426-9436.

Braatz, D. R. (2002). Advanced control of crystallization processes. *Annual Reviews in Control 26*, 87-99.

Braatz, D. R., Hasebe, S. (2002). Particle size and shape control in crystallization processes. In *AIChE Symposium Series: Proceedings of the 6th International Conference on Chemical Process Control*. 307-327.

Chen, C. P. J. (2000). *Cane Sugar Handbook: A Manual for Cane Sugar Manufacturers and Their Chemists*. Noriega LIMUSA.

Chianese, A., Kramer, M. J. H. (2012). *Industrial Crystallization Process Monitoring and Control*. WILEY-VCH.

Choong, K. L., Smith, R. (2004). Novel strategies for optimization of batch, semi-batch and heating/cooling evaporative crystallization. *Chemical Engineering Science 59*, 329-343.

Córdova P. N. M. (2004). Determination of the seed conditions to maximize the growth of particles obtained by batch cooling crystallization. Master Thesis, Instituto Tecnológico de Orizaba. Orizaba, Veracruz, México.

Damour, C., Benne, M., Boillereaux, L., Grondin-Perez, B., Chabriat, J. P. (2011). Multivariable linearizing control of an industrial sugar crystallization process. *Journal of Process Control 21*, 46-54.

Fujiwara, M., Nagy, Z. K., Chew, J. W., Braatz, R. D. (2005). First- principles and direct design approaches for the control of pharmaceutical crystallization. *Journal of Process Control 15*, 493-504.

Georgieva, P., Meireles, M. J., Feyo de Azevedo, S. (2003). Knowledge-based hybrid modelling of a batch crystallisation when accounting for nucleation, growth and agglomeration phenomena. *Chemical Engineering Science 58*, 3699-3713.

Gerstlauer, A., Motz, S., Mitrović, A., Gilles, E. D. (2002). Development, analysis and validation of population models for continuous and batch crystallizers. *Chemical Engineering Science 57*, 4311-4327.

Hanks, J. (1997). Counting Particles of Cells using IMAQ Vision; Application Note 107; National Instruments, Inc.: Austin, TX.

Harrop, K. L., Spanfelne, W. H., Jahoda, M., Otomo, N., Etchelles, A. W., Bujalski, W., Nienow, A. W. (1997). Impact of suspended solids on the homogenisation of the liquid phase under turbulent conditions in a stirred vessel. *Recents Progress an Genie des Procedes 11*, 41-48.

Hermanto, M.W., Chiu, M.S., Woo, X.Y., Braatz, R. D. (2007). Robust optimal control of polymorphic transformation in batch crystallization. *AIChE Journal 53*, 2643-2650.

Hojjati, H., Sheikhzadeh, M., Rohani S. (2013). Control of supersaturation in a semibatch antisolvent crystallization process using a fuzzy logic controller. *Industrial and Engineering Chemistry Research 46*, 1232-1240.

Hu, Q., Rohani, S., Jutan, A. (2005). Modelling and optimization of seeded batch crystallizers. *Computers and Chemical Engineering 29*, 911-918.

Kaćunić, A., Akrap, M., Kuzmanić, N. (2013). Effect of impeller type and position in a batch cooling crystallizer on the growth of borax decahydrate crystals. *Chemical Engineering Research and Design 91*, 274-285.

Kalbasenka, A., Huesman, A., Kramer, H. (2011). Modeling batch crystallization processes: Assumption verification and improvement of the parameter estimation quality through empirical experiment design. *Chemical Engineering Science 66*, 4867-4877.

Kalbasenka, A., Huesman, A., Kramer, H. (2004). Impeller frequency as a process actuator in suspension crystallization of inorganic salts from aqueous solutions. In: *11th International Workshop on Industrial Crystallization*. 135-143.

Khaddour, A. I., Bento, M. S. L., Ferreira, A. M. A., Rocha, N. A. F. (2010). Kinetics and thermodynamics of sucrose crystallization from pure solution at different initial supersaturations. *Surface Science 604*, 1208-1214.

Kim, D. Y.; Yang, D. R. (2013). A novel method for measurement of crystal growth rate. *Journal Crystal Growth 373*, 54-58.

Kim, Y. H., Lee, K., Koo, K. K., Shul, Y. G., Haam, S. (2002). Comparison study of mixing effect on batch cooling crystallization of 3-Nitro-1,2,4-triazol-5-one (NTO) using mechanical stirrer and ultrasound irradiation. *Crystal Research Technology 37*, 928-944.

Madras, G., McCoy, B. J. (2007). A fragmentation model for crystal attrition. *Journal of Crystal Growth 305*, 211-217.

Mersmann, A. (2001). *Crystallization Technology Handbook*. M. Dekker, Ed. Second Edition. New York, USA.

Mersmann, A., Braun, B., Löffelmann, M. (2002). Prediction of crystallization coefficients of the population balance. *Chemical Engineering Science 57*, 4267-4275.

Mesbah, A., Landlust, J., Versteeg, C., Huesman, A. E. M., Kramer, H. J. M., Ludlage, J. H. A, Van den Hof, P. M. J. (2010). Model-based optimal control of industrial batch crystallizers. *Proceedings of the 20th European Symposium on Computer Aided Process Engineering*; Elsevier B.V. 1563-1568.

Mesbah, A., Landlust, J., Huesman, A. E. M., Kramer, H. J. M., Jansen, P. J., Van den Hof, P. M. J. (2010). A model-based control framework for industrial batch crystallization processes. *Chemical Engineering Research and Design 88*, 1223-1233.

Mesbah, A., Nagy, Z. K., Huesman, M. E., Kramer, H. J. K., Van den Hof, J. M. P. (2012). Nonlinear model-based control of a semi-industrial batch crystallizer using a population balance modeling framework. *IEEE Transactions of Control Systems Technology 20*, 1188-1201.

Mitchell, A. N., Ó'Ciardhá, T. Clifford., Frawley, J. P. (2011). Estimation of the growth kinetics for the cooling crystallization of paracetamol and ethanol solutions. *Journal of Crystal Growth 328*, 39-49.

Myronchuk, V., Yeshchenko, O., Samilyk, M. (2013). Sucrose cooling crystallization modelling. *Journal of Faculty of Food Engineering 12*, 109-114.

Nagy, Z. K. (2009). Model based robust control approach for batch crystallization product design. *Computers and Chemical Engineering 33*, 1685-1691.

Nagy, Z., Aamir, E. (2012). Systematic design of supersaturation controlled crystallization processes for shaping the crystal size distribution using an analytical estimator. *Chemical Engineering Science 84*, 656-670.

Nagy, Z. K., Fujiwara, M., Braatz, R.D. (2008). Modelling and control of combined cooling and antisolvent crystallization processes. *Journal of Process Control 18*, 856-864.

Ni, X., Liao, A. (2010). Effects of mixing, seeding, material of baffles and final temperature on solution crystallization of L-glutamic acid in an oscillatory baffled crystallizer. *Chemical Engineering Journal 156*, 226-233.

Qamar, S., Hussain, Iltaf., Seidel-Morgenstern, A. (2011). Application of discontinuous Galerkin scheme to batch crystallization models. *Industrial and Engineering Chemistry Research 50*, 4113-4122.

Quintana-Hernández, P., Bolaños-Reynoso, E., Miranda, C.B., Salcedo, E. L. (2004) Mathematical modeling and kinetic parameter estimation in batch crystallization. *AIChE Journal 50*, 1407-1417.

Quintana-Hernández, P. A., Díaz-Pérez G., Rico-Ramírez V., Salcedo-Estrada, L. I. (2016). Metastable zone width measurement of adipic acid-water solutions. *Revista Mexicana de Ingeniería Química 15*, 1009-1018.

Quintana-Hernández, P. A., Moncada-Abaunza, D. A., Bolaños-Reynoso, E., Salcedo-Estrada, L. I. (2005). Evaluation of sugar crystal growth and determination of surface shape factor. *Revista Mexicana de Ingeniería Química 4*, 123-129.

Quintana-Hernández, P. A., Uribe, Martinez. B., Rico, R. V., Bolaños, R. E. (2008). Comparative analysis of power low type and diffusion-integration kinetic equations in batch cooling of sugar cane. *Revista Mexicana de Ingeniería Química 7*, 171-182.

Sánchez-Sánchez. K. B., Bolaños-Reynoso, E., Galicia-Contreras, L. S., Li, J., Quintana-Hernández, P. A. (2015). Effects of agitation rate on the metastable zone width in sugar cane batch crystallization. *XXXVI AMIDIQ's Memories*, México.

Sander, A., Kardum, P. (2012). Pentaerythritol crystallization. Influence of the process conditions on the granulometric properties of crystals. *Advanced Powder Technology 23*, 191-198.

Sarkar, D., Rohani, S., Jutan, A. (2006). Multi-objective optimization of seeded batch crystallization processes. *Chemical Engineering Science 61*, 5282-5295.

Suarez, P. L. A., Georgieva, P., Feyo de Azevedo, S. (2011). Nonlinear MPC for fed-batch multiple stages sugar crystallization. *Chemical Engineering Research & Development 89*, 753-767.

Swindells, J. F., Snyder, C. F., Hardy, R. C., Golden, P. E. (1958). Viscosities of sucrose at various temperatures: tables of recalculated values. UNITED STATES DEPARTMENT OF COMMERCE, National Bureau of Standards.

Velazquez, C. O., Bolaños, R. E., Rodriguez, E., Alvarez, R. J. (2010). Characterization of cane sugar crystallization using image fractal analysis. *Journal of Food Engineering 100*, 77-84.

Velazquez, C. O., Bolaños, R. E., Rodriguez, E., Alvarez, R. J. (2010). Fractal analysis of crystallization slurry images. *Journal of Crystal Growth 312*, 842-850.

Velazquez, C. O., Bolaños, R. E., Lopez, Z. L., Alvarez, R. J. (2010). Experimental evaluation of the concentration zone widths in cane sugar crystallization using data and image acquisition. In *Proceedings of the World Congress on Engineering*, London, U. K.

Wang, Y. H., Ward, D. F. (2015). Seeding and optimization of batch reactive crystallization. *Industrial and Engineering Chemistry Research 54*, 9360-9368.